JOURNAL OF GEOPHYSICAL RESEARCH, VOL. 100, NO. E6, PAGES 11,709–11,718, JUNE 25, 1995

Self-affine (fractal) topography: Surface parameterization and radar scattering

Michael K. Shepard[1]
Center for Earth and Planetary Studies, National Air and Space Museum, Smithsonian Institution, Washington, D.C.

Robert A. Brackett and Raymond E. Arvidson
Department of Earth and Planetary Sciences, Washington University, Saint Louis, Missouri

Abstract. Starting with the assumption that planetary surfaces are self-affine (fractal) over the scales applicable to radar scattering, we derive various surface parameters, e.g., rms slopes and autocorrelation functions, and examine the implications for radar scattering models. The results of this work provide several new insights of interest to planetary geologists and others using radar to study surface features. First, the unidirectional slope histograms of self-affine surfaces are Gaussian, and the adirectional slope histograms are Rayleigh. Normalization of the adirectional histogram by solid angle results in a Gaussian adirectional slope density function and therefore a Gaussian quasi-specular angular scattering function. Next, the wavelength dependent behavior of surface roughness inferred from lunar radar observations is consistent with self-affine topography. Finally, surface rms height measurements are functions of profile length. Therefore, when determining the applicability of the small perturbation model to a surface based on those measurements, it is necessary to consider the length of the profile with respect to the sampling wavelength.

1. Introduction

Radar remote sensing provides a significant source of our information about the topography and texture of planetary surfaces. A large body of recent work has demonstrated that many surfaces are described by self-affine or fractal statistics over a wide range of scales, i.e., micrometers to kilometers [cf. *Mandelbrot*, 1982; *Turcotte*, 1992]. The purpose of this paper is twofold: (1) to examine how self-affine statistics translate into more commonly used surface roughness parameters like unidirectional and adirectional rms slope distributions, rms height, autocorrelation length, and effective slope; and (2) to explore some implications of self-affine topography for radar scattering models. In this work, we consider only monofractal behavior, i.e., behavior described by a single fractal dimension.

The paper is divided into five sections, this introduction being the first. Section two reviews the definitions of terms used throughout this paper and discusses the generation and measurement of fractal profiles and surfaces. The third section uses fractal theory to derive the behavior of commonly used surface parameters, including the autocorrelation function and various surface slope distributions. In section four, several radar scattering problems are examined in light of these theoretical considerations, including a discussion of quasi-specular angular scattering functions, the wavelength dependence of scattering, and a note on the application of the small perturbation model. Finally, section five summarizes our results.

Throughout this paper, examples from both real and synthetic surfaces are given to foster an intuitive sense of topographic description and the concepts discussed. However, we are working with a system which is described only in terms of statistical parameters. Whereas the behavior of a large collection of topographic profiles will conform with theoretical expectations, any single profile or segment of a profile often will not. Therefore, in order to be succinct and illustrative, we have chosen examples which display behavior typical of the larger, i.e., theoretical, population.

2. Fractal Basics

2.1. Assumptions and Definitions

Although the term fractal is often used to mean either self-affine or self-similar, in this paper we limit its use to mean self-affine. We assume that natural surfaces are self-affine over scales applicable to microwave scattering, i.e., centimeters to hundreds of meters. For surfaces, we use the coordinate axes x and y to refer to horizontal directions and z for the vertical direction. For profiles, we use x for the horizontal direction and z for the vertical direction. We use angle brackets to indicate the expectation or average value of a quantity. For clarity, we review the definitions of a few terms that will be used in the remaining discussion.

1. Self-affinity. The scaling behavior of a topographic surface such that increasing the scale of the x and y axes by a factor r must be compensated for in the z direction by a factor r^H for the surface to remain statistically identical. The term H

[1]Now at Department of Geography and Earth Science, Bloomsburg University, Bloomsburg, Pennsylvania.

Paper number 95JE00664.
0148-0227/95/95JE-00664$5.00

is known as the Hurst exponent [*Hastings and Sugihara*, 1993] and sometimes referred to as the Hausdorff measure [*Falconer*, 1990; *Turcotte*, 1992], $0 < H < 1$. The term self-similar corresponds to the special case of $H = 1$ [Power and Tullis, 1991].

2. Fractal dimension. For a self-affine surface, the fractal dimension $D = 3 - H$; for a cross-sectional profile through a self-affine surface, $D = 2 - H$.

3. Ordinary Brownian noise (oBn). Self-affine behavior with $H = 0.5$. Also referred to as a "random walk."

4. Fractional Brownian noise (fBn). Self-affine behavior, $0 < H < 1$.

5. Variance (σ^2). The variance of all points on a surface or profile about the mean value:

$$\sigma^2 = \langle [z - \bar{z}]^2 \rangle \quad (1)$$

6. The rms height (σ). The square root of the variance.

7. Allan variance (υ^2). The (height) variance of the population of points on a surface or profile separated by a distance (Δx,Δy) [*Allan*, 1966]:

$$\upsilon^2 = \langle [z(x,y) - z(x + \Delta x, y + \Delta y)]^2 \rangle \quad (2)$$

In many fractal texts, the Allan variance is often referred to as simply the variance. We have separated these terms here to avoid confusion later. The Allan variance is also known as the structure function [*Ogilvy*, 1991] and variogram [*Mark and Aronson*, 1984; *Chase*, 1992]. Strictly speaking, the Allan variance is a vector function, i.e., dependent on the direction of Δx and Δy. However, a common assumption in scattering models is that the surface is isotropic; therefore we have written (2) in its simpler scalar form.

8. Allan deviation (υ). The square root of the Allan variance.

9. Slope histogram ($P(s) = P(\tan\theta)$). A function describing the frequency or number of slopes within any angular interval. Note that s is the slope or tangent of the slope angle θ.

10. Slope density function or slope distribution ($p(s) = p(\tan\theta)$). A function describing the frequency or number of slopes within any solid-angle interval. The slope density function is essentially the slope histogram normalized by solid angle. The difference will become apparent when unidirectional and adirectional slope distributions are discussed.

2.2. Ordinary Brownian Noise

Ordinary Brownian noise (oBn) (D=1.5 for profiles, 2.5 for surfaces) or a "random walk" is a continuous but nondifferentiable function. It can be generated in several ways. One of the simplest methods is to start on a horizontal axis, move in incremental steps along the x axis, and at every increment take a (vertical) step up or down [*Turcotte*, 1992]. The limit of this process as step-size goes to zero is Brownian noise [*Hastings and Sugihara*, 1993]. Another method involves integrating a Gaussian white noise spectrum [*Voss*, 1988].

There are several important properties of oBn which will be used extensively throughout this paper. For any incremental step, Δx, the population of height differences $\Delta z(x) = z(x + \Delta x) - z(x)$ have the following properties: (1) the mean, $\langle \Delta z \rangle$, is zero; (2) the Allan variance, $\langle \Delta z^2 \rangle = \upsilon^2$ is proportional to the step size, Δx, used to measure a profile

$$\upsilon^2 = c^2 \Delta x \quad (3)$$

where c^2 is a constant of proportionality; (3) the increments Δz are distributed according to Gaussian statistics; (4) the increments Δz are uncorrelated; and (5) the magnitude of z is arbitrary – in fact, x and z are not even required to have the same units [Hastings and Sugihara, 1993]. If Δx is taken to be the length of the profile, L, then (3) also states that the Allan variance is proportional to the length of the profile.

Sayles and Thomas [1978] note that oBn is a nonstationary random process. A stationary process is one in which the properties of any given segment (or area) are statistically identical to any other segment or to the whole. However, oBn is stationary in a more restricted sense, in that segments of the same length (or area) are statistically identical to other segments (or areas) of the same size, but not to segments or areas of different sizes. This restricted sense of stationarity has important ramifications, to be discussed later.

Figure 1 shows a profile of oBn generated using a random walk algorithm and a topographic profile (acquired using helicopter stereophotography [cf. *Farr*, 1992]) of the Black Rock lava flow, Lunar Crater Volcanic Field, Nevada [*Arvidson et al.*, 1991]. The two profiles are statistically the same, and as we will show later, have the same fractal dimension.

2.3. Fractional Brownian Noise

Fractional Brownian noise (fBn) is the general case of self-affine behavior and permits fractal dimensions $1.0 < D < 2.0$ for profiles and $2.0 < D < 3.0$ for surfaces. The properties of fBn are similar to oBn above except that the Allan variance (3) is now given by

$$\upsilon^2 = c^2(\Delta x)^{2H} \quad (4)$$

where H is the Hurst exponent [*Hastings and Sugihara*,

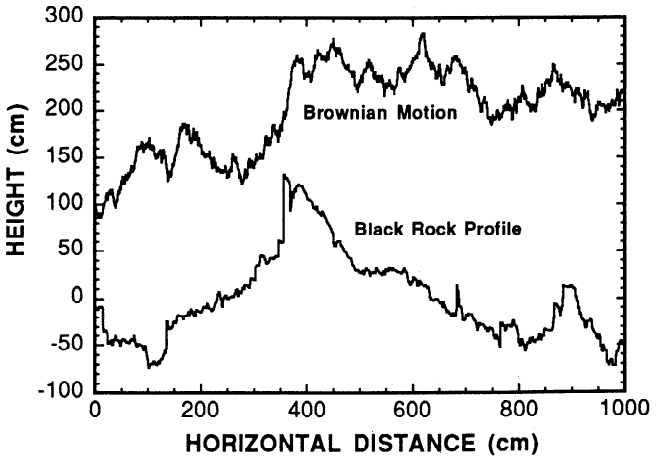

Figure 1. Plot of ordinary Brownian motion or "random walk" (top curve) and a profile of the Black Rock basalt flow (bottom curve). Both figures have a fractal dimension, D = 1.5. The oBn plot is offset for clarity. The Black Rock profile was measured using helicopter stereophotography [cf. *Farr*, 1992]. Data points are 1 cm apart and vertical errors are up to ±4 mm [*Farr*, 1992].

1993]. Comparing (4) with (3) illustrates that $H = 0.5$ for oBn. Furthermore, oBn property (4) above is not generally true for fBn. For $H > 0.5$, adjacent Δz are positively correlated, i.e., a trend in the upward direction tends to remain in that direction, while for $H < 0.5$, adjacent Δz are negatively correlated [*Hastings and Sugihara*, 1993]. The visual effect of this property is that surfaces with $H > 0.5$ ($D < 2.5$) tend to look more "smooth", while surfaces with $H < 0.5$ ($D > 2.5$) tend to look more "rough."

2.4. Scaling Properties of the Variance and rms Height

Our discussion so far has concentrated on properties of the Allan variance and deviation. The behavior of the variance and rms height of a surface or profile will be similar to that of the Allan variance and deviation, but with a subtle difference. Equations (3) and (4) have emphasized that the Allan variance and deviation increase with increasing scale size, Δx. Interestingly though, for a given profile length the variance and rms height will be independent of the scale, Δx, used to measure them. However, if the profile length is varied, the variance and rms height will vary in accordance with (4), where Δx is replaced by the profile length, L. Note also that the proportionality constant, c, will be different from that used in the Allan variance. We will discuss the relationship between these quantities in more detail below.

2.5. Measurement of Fractal Dimension

There are many methods of measuring the fractal dimension of surfaces. One of the first and most intuitive methods used involves plotting the length of a profile as a function of the ruler size used to measure it [*Mandelbrot*, 1982]. There are variations on this method, including counting the number of boxes or circles of a certain size needed to cover a profile [cf. *Voss*, 1988]. In this paper, we utilize two different methods: the power spectrum method [cf. *Voss*, 1988; *Turcotte*, 1992] and the variogram method [cf. *Mark and Aronson*, 1984; *Chase*, 1992]. We use these methods because, in addition to calculating the fractal dimension, they describe the behavior of other statistical parameters.

Power spectrum method. The power spectrum method is often used for both determining the fractal dimension of a surface or profile and synthesizing a fractal surface or profile. Essentially, the power spectrum is a function that defines the amplitude of a given spatial frequency. For a profile, it is defined as

$$S(f) = \frac{1}{L}|X(f,L)|^2 \qquad (5)$$

where S is the power spectral density function, f is the spatial frequency, L is the length of the profile, and X is the Fourier transform of the profile [*Turcotte*, 1992]. A fractal surface can be defined as one with a linear power spectrum (in log-log space), defined by $S = \beta f + \alpha$, where β is the slope ($-3 < \beta \leq -2$) and α is the intercept. Note the units for a profile with height and length measured in meters: X is in m^2 and L is in meters so that S is in m^4m^{-1} or m^3. The variance can be defined as the total area under the power spectrum [*Sayles and Thomas*, 1978; *Ogilvy*, 1991]. The slope of the power spectrum for a profile is related to the fractal dimension by [*Turcotte*, 1992]:

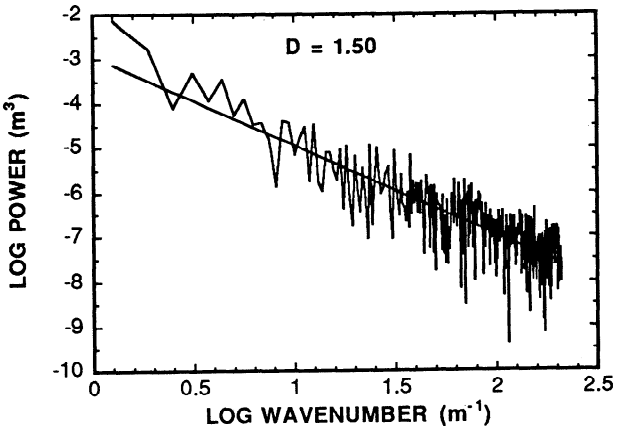

Figure 2. Power spectrum of the Black Rock profile shown in Figure 1. Slope of the best fit line is –2.01, giving $D = 1.50$.

$$\beta = 2D - 5 \qquad (6)$$

Note that the limits of β correspond to limits of $1 < D \leq 1.5$. Determination of fractal dimensions higher than 1.5 using the power spectral method are to be made with caution because of the possible effects of overhangs [*Brown and Scholz*, 1985]. An example of the power spectrum from a profile of the Black Rock a'a flow surface is shown in Figure 2, with a corresponding fractal dimension $D = 1.50$.

Variogram. Another common method of measuring the fractal dimension of a surface or profile is the variogram method [e.g., *Mark and Aronson*, 1984; *Chase*, 1992]. Recall that the variogram is equivalent to the Allan variance (2). Therefore, on a variogram, fBn is represented by (4) [*Mark and Aronson*, 1984]. When plotted on log-log axes, the variogram is linear with slope equal to $2H$. Figure 3 shows the variogram of the Black Rock a'a profile. The fractal dimension from the variogram is 1.48, quite close to the power spectral determination of 1.50.

Comparison of methods. There is an ongoing debate about the use of the power spectrum method for quantifying the fractal dimension. Work relying on the power spectrum method often reports fractal dimensions of ~2.5 for surfaces and ~1.5 for profiles [*Huang and Turcotte*, 1989, 1990; *Farr*,

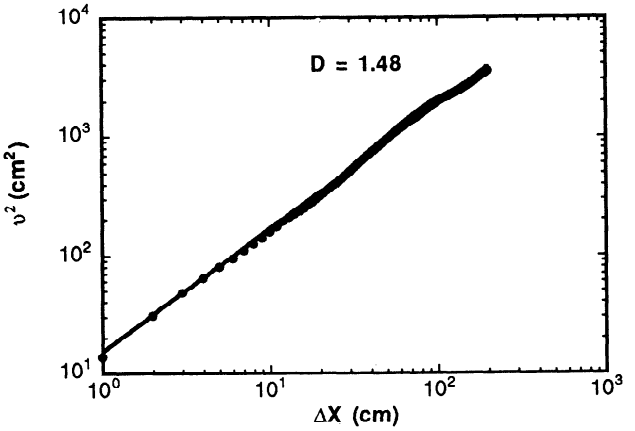

Figure 3. Variogram of Black Rock profile shown in Figure 1. Slope of best fit line is 1.04 giving $D = 1.48$, quite close to the power spectrum determination of $D = 1.50$.

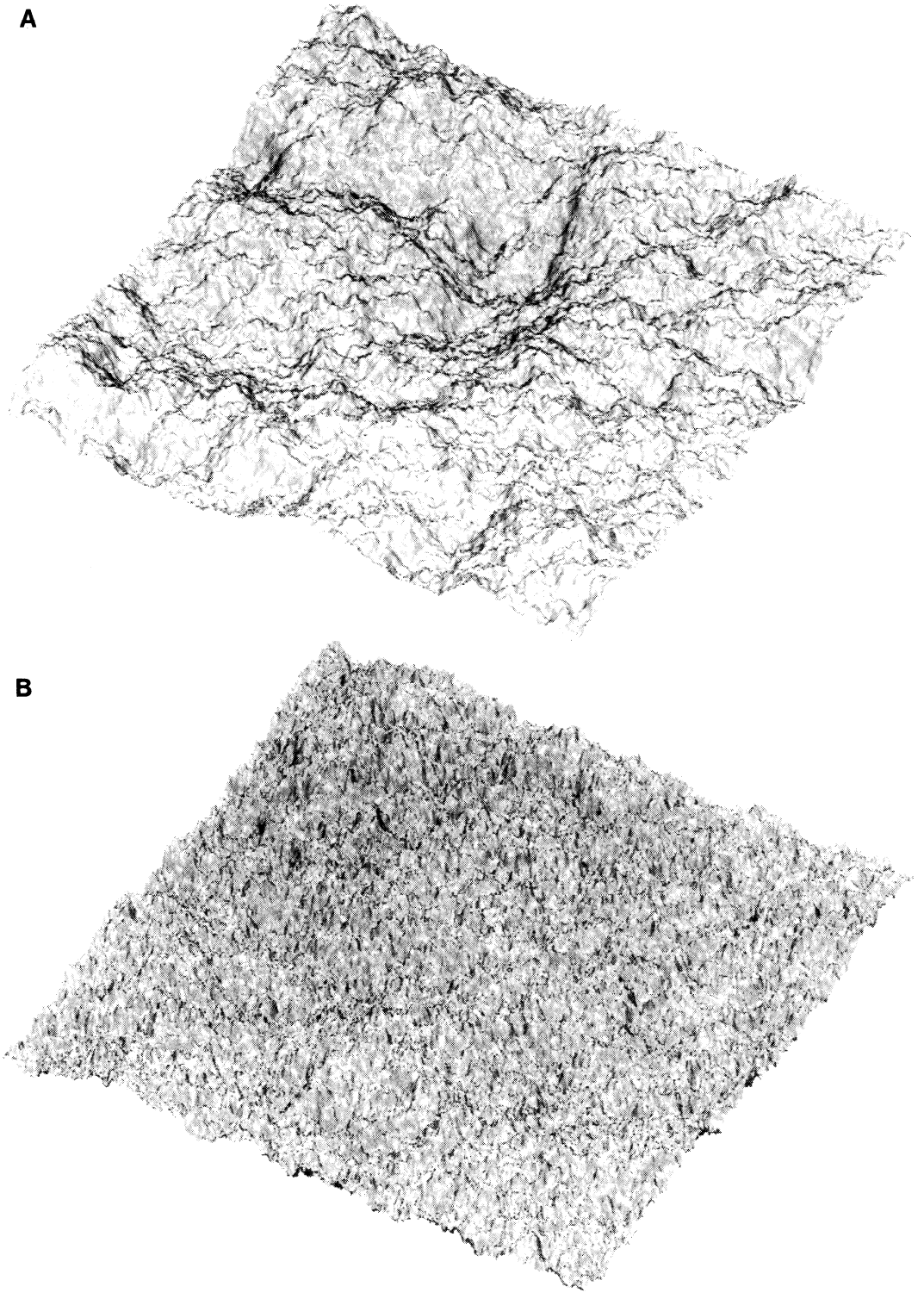

Figure 4. (a) Synthetic fractal surface, D = 2.2, area 512 m x 512 m, point spacing 1 m, rms height of 4 m. (b) Synthetic surface, D=1.5, area of 512m x 512m, rms height of 3.3 m. This surface is statistically identical to the Black Rock flow topography. Vertical exaggeration for both figures is 10x.

1992]. However, work using the variogram method more often reports lower fractal dimensions, typically 2.1-2.3 for surfaces and 1.1-1.3 for profiles, especially at scales of centimeters to hundreds of meters [e.g., *Mark and Aronson*, 1984; *Chase*, 1992]. For comparison, Figure 4 shows two synthetic surfaces with fractal dimensions of 2.2 and 2.5 generated using the power spectrum method [*Voss*, 1988; *Turcotte*, 1992].

Recent work by *Austin et al.* [1994] indicates that determinations of the fractal dimension using the power

spectrum method are biased to slopes of -2.0 (D = 1.5 or 2.5) by spectral leakage (from low frequencies into the higher frequencies). One remedy suggested by *Austin et al.* [1994] is the use of a Hanning filter on the profile or surface prior to computing the power spectrum. We found that filtering out the highest frequency information before the linear regression also improved results. The power spectrum in Figure 2 was generated in this manner.

Our experience leads us to favor the variogram method over the power spectrum method for calculating fractal dimensions from surfaces and profiles. In part, this preference is due to a desire to work with unfiltered data. Also, we find that the variogram is less noisy than the power spectrum (compare Figures 2 and 3). However, for synthesizing fractal surfaces, the power spectrum method is preferred; it is rapid and does not suffer from many of the artifacts that tend to plague spatial methods (cf. *Voss* [1988] for a review of synthesizing algorithms).

2.6. The Role of Scale on Fractal Surfaces

We discuss the role of scale on fractal surfaces through an example. Consider two profiles taken from the same surface. Each profile is a sample of surface height at 1-cm intervals. Profile A is 1000 points long, or 10 m; profile B is 100 points long or 1 m. We assume for simplicity that the mean of the surface heights is zero, that each profile has a fractal dimension of 1.5 corresponding to oBn, and that the profiles were produced with the same random walk algorithm (this latter assumption is equivalent to stating that profile B is a subset of profile A). The rms height of profile A we designate σ_A, and profile B is σ_B. Because our profiles are oBn and produced by the same algorithm, the rms heights are proportional to the square root of profile length (section 2.4 and (3)). Therefore, the relationship between σ_A and σ_B is:

$$\sigma_A = \left(\frac{10\text{m}}{1\text{m}}\right)^{1/2} \sigma_B = (3.16)\sigma_B \tag{7}$$

Comparing the power spectra of profiles A and B, we find that the slope and intercept will be identical. Examination of (5) reveals why. The amplitudes of the Fourier transform of profile A will be $\sqrt{10}$ = 3.16 times higher than profile B because on average, profile A has an rms height 3.16 times larger than B. However, the length of profile A is 10 times longer than B. So the longer profile ($1/L$ term) exactly offsets the amplitude square (X^2) term, resulting in similar power spectral density functions. The only discernible difference will be the existence of more low-frequency terms in the A profile spectrum.

Now multiply the heights of profile B by 3.16 and designate this profile C. The rms height of C is equal to that of profile A. Examination of the power spectrum of C reveals the same slope, i.e., the fractal dimension of C is still 1.5. As discussed earlier (section 2.2, property (5)), the magnitude of the z axis units have no effect on the fractal dimension. However, the intercept of the power spectrum changes in proportion to the height magnification squared, i.e., by a factor of 10. Therefore, although A and C have the same rms height and fractal dimension, they are statistically different, as evidenced by the different power spectra. This difference will manifest itself through the Allan variance and rms slope values, to be discussed below.

3. Fractal Surface Parameters

3.1. Autocorrelation Functions: Background

The autocorrelation function of a profile or surface relates the correlation (or normalized covariance) between points separated by a distance, Δx. If $\Delta x = 0$, the points being compared are the same and the autocorrelation function has a value of 1.0. As Δx is increased, points are generally less correlated, and the function value decreases. The autocorrelation functions most often assumed for surfaces are the Gaussian

$$\rho(\Delta x) = exp\left(-\frac{\Delta x^2}{l^2}\right) \tag{8}$$

and exponential

$$\rho(\Delta x) = exp\left(-\frac{|\Delta x|}{l}\right) \tag{9}$$

functions (cf. *Ogilvy* [1991] for a discussion of these and other functions). The variable l is the autocorrelation length, defined as the distance over which the autocorrelation function decreases to a value of $1/e$ or ~0.37.

An important property of any autocorrelation function is the behavior of its derivative at the origin. Examination of (8) and (9) reveals that the Gaussian function has a continuous derivative at the origin, while the exponential function has a discontinuous derivative, i.e., the value of the derivative is different, depending upon whether the origin is approached from the positive or negative side. This difference makes the Gaussian function easier to manipulate mathematically.

3.2. Autocorrelation Functions of Fractal Surfaces

One method of calculating the autocorrelation function of a sample set is to take the inverse Fourier transform of the power spectral density function [*Falconer*, 1990]. However, we choose to calculate the autocorrelation function of fBn with the variogram because of its simplicity and intuitive nature. Because any given finite segment of a fractal surface is stationary, i.e., the statistical properties of similar length segments are identical, the variogram and covariance are related by

$$v^2(\Delta x) = k\left[\sigma^2 - \text{Cov}(\Delta x)\right] \tag{10}$$

where σ^2 is the variance, k is a constant, and Cov(Δx) is the (auto)covariance between points Δx apart [*Jupp et al.*, 1988; *Falconer*, 1990]. For stationary functions, *Jupp et al.* [1988] show that k=2. When $\Delta x = 0$, the variogram is zero, i.e., the points being compared are identical. As $\Delta x \rightarrow \infty$, Cov($\Delta x$) $\rightarrow$ 0, i.e., the profiles are uncorrelated and $v^2 = k\sigma^2$.

The autocorrelation function, $\rho(\Delta x)$, is the normalized (auto)covariance of that function:

$$\rho(\Delta x) = \frac{\text{Cov}(\Delta x)}{\sigma^2} \tag{11}$$

Substituting (11) and (4) into (10) and rearranging terms, we obtain

$$\rho(\Delta x) = 1 - \frac{c^2}{k\sigma^2}|\Delta x|^{2H} \tag{12}$$

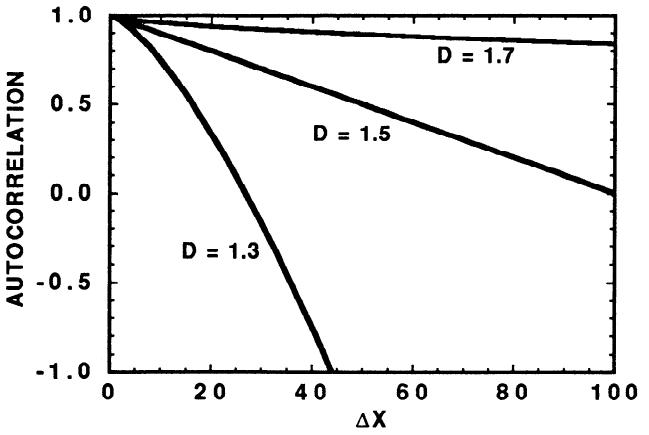

Figure 5. Autocorrelation functions of fractal profiles, given by Eq. (12). The term $c^2/k\sigma^2$ is kept constant (0.01) to facilitate comparisons of the autocorrelation functions between the different fractal dimensions.

A similar derivation of (12) is given by *Falconer* [1990].

Compare the behavior of (12) at the origin with the Gaussian and exponential functions. For "smooth" surfaces (i.e., $D < 2.5$, $H > 0.5$), the derivative is continuous at the origin, similar to the Gaussian function. However, for "rough" surfaces (i.e., $D > 2.5$, $H < 0.5$), the derivative is discontinuous, similar to the exponential function. Furthermore, *Ogilvy* [1991] notes that surfaces with exponential autocorrelation functions have more high-frequency terms than those with Gaussian autocorrelation functions, mirroring the behavior of the analogous fractal autocorrelation functions.

Figure 5 illustrates the behavior of (12) for three cases of fractal behavior: $D = 1.3$, 1.5, and 1.7. Figure 6 shows the autocorrelation function of the Black Rock profile (Figure 1). There are obvious differences between the theoretical and observed behavior. Whereas the Gaussian, exponential, and fractal autocorrelation functions monotonically decrease with distance, real surfaces often show periodicities, crossing the x axis several times. This behavior is reminiscent of the sinc function ($\sin(x)/x$). The similarity is not coincidence. A sinc function is the result of sampling an infinite time or spatial series with a finite window filter. Similarly, the damped periodic behavior exhibited by the autocorrelation functions of many real surfaces is due to the finite size of the profile.

There is one final and important point to note about fractal surface autocorrelation functions. When using the Gaussian or exponential autocorrelation functions, the surface is assumed to be stationary, as defined earlier (section 2.2). Stationary surfaces have autocorrelation lengths that are independent of the profile length or surface area. However, fractal surfaces are not stationary, except in the limited sense that profiles or areas of the same size are statistically identical. Nonstationary surfaces have autocorrelation functions, and therefore autocorrelation lengths, that are dependent on the profile length or surface area. This can be seen by examining (4) and (12). Therefore, assigning an autocorrelation length to a fractal surface or profile is meaningless unless the scale is considered.

3.3. Slope Distributions of Fractal Surfaces

When modeling the wave scattering properties of planetary surfaces, it is convenient to utilize a parameter related to the distribution of surface slopes. Several types of slope parameters are in common use, the unidirectional slope distribution and rms value, adirectional slope distribution and rms value, and effective slope. We will briefly discuss each of these parameters and then derive their quantitative forms for a fractal surface. To illustrate the distribution forms, we utilize the synthesized surface shown in Figure 4b. This surface was designed to simulate the Black Rock flow and therefore has a fractal dimension of 2.50, area of 512 m x 512 m, and rms height of 3.3 m. Note that the simulated surface has a much higher rms height than the 46 cm measured from our 10-m profile. We have simply scaled the rms height for the larger simulated size using (3). This allows us to compute slope statistics at a 1-m scale with a statistically significant number of data points.

Unidirectional slopes. The unidirectional slope is the rise over run between two points along a linear transect of a surface, i.e., the slope that would be measured from a profile. *Efford* [1990] notes that synthetic fractal surfaces have unidirectional slope histograms that are accurately represented by Gaussian functions.

From the properties listed for oBn and fBn, we note that the difference in heights, Δz, between any two points on a fractal surface has a Gaussian distribution. If we imagine a transect along a horizontal fractal surface from which we measure the change in height, Δz, at uniform intervals, Δx, then the slopes derived from these measurements, $\Delta z/\Delta x$, will also have a Gaussian distribution. Therefore, the unidirectional slope distribution of a fractal surface is Gaussian, with (slope) variance $\langle(\Delta z/\Delta x)^2\rangle$. The rms slope is just the square root of this variance and is typically converted to degrees by taking the inverse tangent. Figure 7a shows a histogram of the unidirectional slopes of the surface in Figure 4b measured with a Δx of 1 m. The curve is fit by a Gaussian with $s_{rms} = 0.60$ ($\theta_{rms} = 31°$).

A note on terminology is in order. Figure 7a shows the undirectional slope distribution with the x axis in terms of slope, i.e., rise/run, and not in degrees or radians. If the x axis is in terms of degrees or radians, we prefer the term unidirectional slope angle distribution. Although a seemingly trivial distinction, the unidirectional slope angle distribution of a fractal surface will not be Gaussian, except in the limit as $\theta_{rms} \to 0$. This is because the inverse tangent is increasingly nonlinear at higher slopes.

Adirectional slopes. The adirectional slope is the tangent of the angle between a surface normal and the

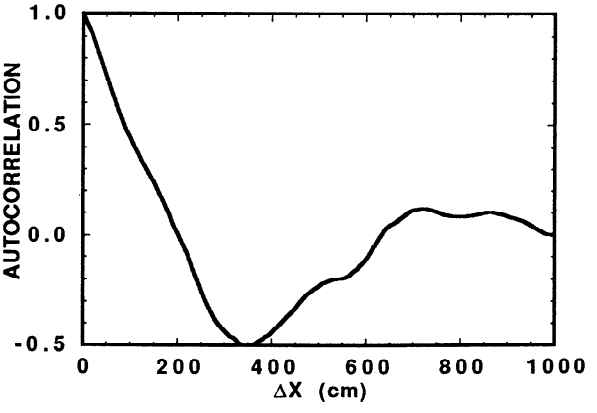

Figure 6. Autocorrelation function of the Black Rock profile shown in Figure 1.

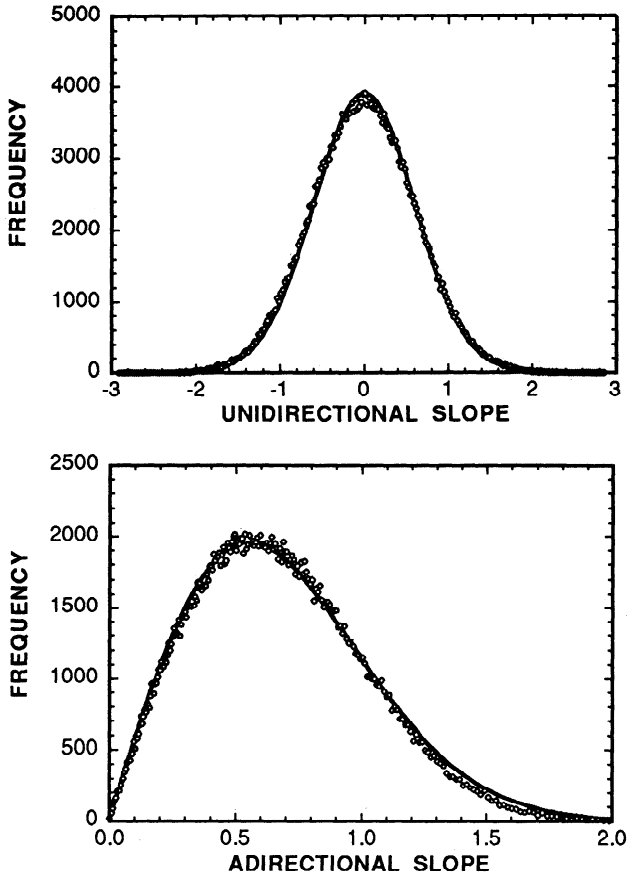

Figure 7. (a) Unidirectional slope distributions of Figure 5b (circles). Curve is best fit Gaussian, tan θ_{rms} = 0.60 (θ_{rms} = 31°). (b) Adirectional slope distributions of Figure 6b (circles). Curve is best fit Rayleigh, mode at 0.56 (29°).

vertical. Initially, one might think the adirectional slope histogram to be of the same form as the unidirectional slope histogram. However, examination of Figure 7b, a histogram of adirectional slopes for the surface in Figure 4b, shows this not to be the case. The histogram shown in Figure 7b is best fit by a Rayleigh function, defined by

$$P(s) = \frac{s}{s_0^2} e^{-(s^2/2s_0^2)} \tag{13}$$

where P is the slope histogram function, s is the slope of the surface normal polar angle, and s_0 is the mode of the distribution, equal to the unidirectional slope rms slope. In Fig. 7b, the best fit Rayleigh to our synthetic surface gives s_0 = 0.56 (θ_0 = 29°), very close to the unidirectional value of 0.60. Interestingly, field measurements of geologic surfaces have adirectional slope histograms similar to the Rayleigh distribution [*McCollom and Jakosky*, 1993].

The Rayleigh histogram of slopes follows directly from the behavior of surfaces with Gaussian unidirectional slope histograms. A Rayleigh function is effectively the sum of two Gaussian functions in quadrature [*Beckman*, 1963]. This may be visualized as follows. Imagine two orthogonal transects along some surface, the unidirectional slope distribution of each being Gaussian. At every point on the surface, the adirectional slope, s_{adir}, for that point can be approximated by

$$s_{adir} = \left(\Delta z_x^2 + \Delta z_y^2\right)^{1/2} \tag{14}$$

where Δz_x is the vertical change in the x direction, Δz_y is the vertical change in the y direction, and we have assumed the horizontal distance between points is 1.0. From (14) it is apparent that the adirectional slope will always be greater than or equal to the maximum of Δz_x or Δz_y. Since it is unlikely that zero slopes along one direction will coincide with zero slopes in the orthogonal direction, the mode of the resulting function will be nonzero. This is responsible for the skewed nature of the Rayleigh function.

In radar scattering studies, the parameter that must be utilized is the adirectional slope histogram normalized to solid angle, also known as the adirectional surface slope density function (see 2.1, definition 10) [*Simpson and Tyler*, 1982; *Campbell and Garvin*, 1993; *McCollom and Jakosky*, 1993]. We adopt the nomenclature of *Simpson and Tyler* [1982] to express our normalized function. Our synthetic surfaces are generated so that the projected surface area of each facet is a constant; we therefore utilize the modified Rea, Hetherington, and Mifflin probability density function, $p_{RHM'}(\theta)$ [*Simpson and Tyler*, 1982, equation A5]. The normalization for this function is

$$2\pi \int_0^{\pi/2} p_{RHM'}(\theta) \sin\theta \, d\theta = 1 \tag{15}$$

Normalizing (13) to this form gives

$$p_{RHM}(\theta) = \frac{1}{2\pi \tan^2\theta_{rms}} \sec^3(\theta) e^{-\tan^2\theta / 2\tan^2\theta_{rms}} \tag{16}$$

The secant term arises in part from the conversion of (13) in terms of slope into degrees. Equation (16) is a Gaussian function with rms slope tan(θ_{rms}) [*Simpson and Tyler*, 1982].

The rms slope as a function of scale. We now derive the behavior of the rms slope for a fractal surface sampled at different horizontal scales, Δx. We have defined the rms slope, s_{rms}, as $\sqrt{<(\Delta z/\Delta x)^2>}$. The rms value of Δz will equal υ (the Allan deviation) and from (4), υ is equal to $c(\Delta x)^H$. Therefore, the rms slope can be written as

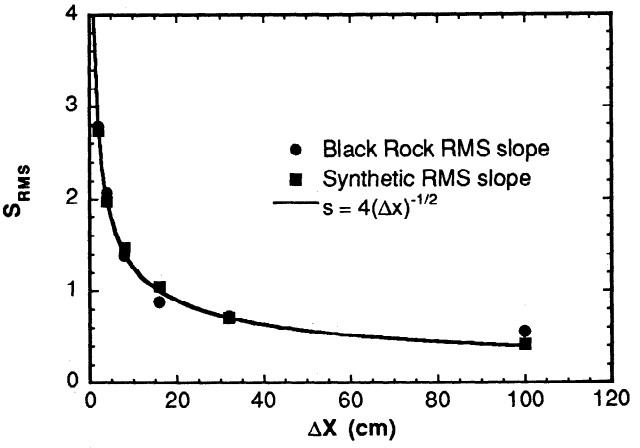

Figure 8. Plot of rms slope versus scale for the Black Rock profile, demonstrating the $\lambda^{-0.5}$ dependence.

$$s_{rms} = \tan \theta_{rms} = \frac{c(\Delta x)^H}{\Delta x} = c(\Delta x)^{H-1} \quad (17)$$

For oBn, $H = 0.5$, and the rms slope will decrease as $1/\sqrt{\Delta x}$.

Figure 8 shows a plot of s_{rms} as a function of scale length Δx for the Black Rock profile and synthetic profile, and a curve with the $c/\sqrt{\Delta x}$ dependence expected from (17). Note that s_{rms} measured at 1 m is 0.56 ($\theta_{rms} = 29°$), in excellent agreement with the value calculated for this scale on our synthetic surface (see Figure 7).

Effective surface slope. We define the effective surface slope following *Campbell and Garvin* [1993] as:

$$s_{EFF} = \frac{\sqrt{2}\,\sigma}{l} \quad (18)$$

where l was defined earlier (section 3.1) as the autocorrelation length [*Hagfors and Evans*, 1968]. Both (18) and (17) are referred to throughout the literature as "rms slope." *Campbell and Garvin* [1993] chose the term "effective slope" to differentiate (18) from (17). We have included the $\sqrt{2}$ following the original form of this function given by *Hagfors and Evans* [1968].

As previously discussed, for fractal surfaces, both l and σ are functions of the profile length and Hurst exponent (sections 2.3, 2.4, and 3.2, (4) and (12)). Therefore, different profile lengths should have different s_{EFF} following the general form of (17) with Δx replaced by profile length L. However, both l and σ are independent of the scale used (sections 2.4 and 3.2). Therefore, for a fractal surface the effective slope is a constant for any given profile length. This behavior was noted by *Campbell and Garvin* [1993] in their topographic analysis of several lava flows.

Relationship of Allan variance and variance. So far, we have primarily discussed the properties of the Allan variance and deviation of points on a profile or surface separated by a distance, Δx. However, the quantities commonly reported on surfaces or profiles are variance and rms height. As mentioned earlier (section 2.4), the variance and rms height follow the general fractal scaling law (4) but with constants different from the Allan variance, and with the term Δx replaced with the profile length L. According to (10), when considering an area or profile as a whole, the following relationship should exist between the Allan variance and variance:

$$\upsilon^2 = k\sigma^2 \quad (19)$$

where k is a constant. For stationary functions, $k = 2$. However, our experience with millions of computer simulations indicates that k tends to fall between 4 and 6 for fractal (oBn) profiles, but this value can vary significantly. We have found examples of $k = 25$ or more. The difference between these findings and the theoretical value for stationary functions is apparently due to the more limited stationary properties of fractal behavior, although at this point we cannot be more rigorous.

The significance of (19) is that the rms slopes reported from topographic measurements or radar scattering curves are related to the rms height of the surface, but smaller by a factor of $\sqrt{k}$. For example, consider the Black Rock profile. At 1-m scale, we obtained an rms slope of 0.6. The Allan deviation of 1-m segments is therefore 1 m x 0.6 = 60 cm. However, a calculation of the rms height of 1-m segments from the Black Rock and synthetic profiles averages ~15 cm, 400% smaller. In this case, k~16.

The point of this discussion is to emphasize that the rms height of a surface is related to the rms slope, but only through the intermediate Allan deviation and (19). It is critical to keep this relationship in mind when attempting to interpret radar-derived values of rms slope in terms of surface roughness parameters.

4. Applications to Radar Scattering

4.1 Quasi-Specular Scattering From a Fractal Surface

Quasi-specular models for radar backscatter assume that the surface is composed of a statistical distribution of facets, large and smooth compared with the wavelength of incident power. It is also commonly assumed that only facets oriented with normals coincident with (or within a differential solid angle of) the radar beam contribute to the returned power. Therefore, the parameter that must be utilized in quasi-specular models is the adirectional surface slope density function [*Simpson and Tyler*, 1982; *Campbell and Garvin*, 1993; *McCollom and Jakosky*, 1993]. For a self-affine surface, we have demonstrated that the surface slope density function is Gaussian (16). This can readily be converted into radar cross section [*Simpson and Tyler*, 1982]:

$$\sigma_0 = \frac{A}{\tan^2\theta_{rms}} \sec^4(i) e^{-\tan^2(i)/2\tan^2\theta_{rms}} \quad (20)$$

where A is a proportionality constant and i is the radar incidence angle.

Equation (20) conveniently neglects that, by definition, a self-affine surface will display roughness at scales smaller than the incident wavelength, thus adding a component of diffuse scattering to any return. The modification of (20) to account for this addition is beyond the scope of this paper.

4.2. Relationship of Lunar rms Slope and Radar Wavelength

The rms slopes of planetary surfaces are often calculated by fitting quasi-specular models to angular scattering functions [e.g., *Muhleman*, 1964, *Hagfors and Evans*, 1968, *Simpson and Tyler*, 1982, and numerous others]. All of these models have a parameter which is closely related to the surface rms slope. If planetary surfaces are self-affine, how should rms slope and radar wavelength relate?

To derive this behavior, we assume that (1) the only contribution to the near-nadir radar echo is quasi-specular scattering from the planetary surface, i.e., no significant diffuse or volume scattering component; and (2) the incident radar samples surface features at length scales proportional to its wavelength, i.e., short wavelengths sample smaller portions of the surface than long wavelengths [cf. *Hagfors and Evans*, 1968]. The derivation then leads to a form identical to (17):

$$\theta_{rms} = \tan^{-1}\left[\frac{\upsilon}{n\lambda}\right] = \tan^{-1}\left[K\lambda^{H-1}\right] \quad (21)$$

where n is a constant that relates the size of the wavelength

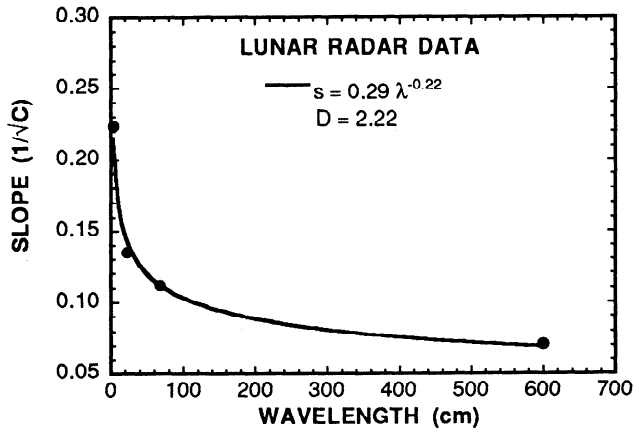

Figure 9. The rms slope versus wavelength, Moon, using Hagfors fits to angular scattering functions. Line is best fit power law, indicating a surface fractal dimension of 2.22. Surface in Figure 4a is statistically identical, assuming rms height of 2 cm over 68-cm profile length.

to the size of the area sampled by the wave, and K is a combination of the constants n and c (4).

Simpson and Tyler [1982] were among the first to observe a power law dependence between radar wavelength and inferred lunar surface roughness. They noted that the power law exponent varies with the terrain and reported best fit exponents (H-1) of 0.0 to -0.42, corresponding to fractal dimensions of 2.0–2.4. *Muhlemann* [1964] noted a logarithmic relationship on the Moon between his roughness parameter, α, and radar wavelength. Although not identical, Muhlemann's logarithmic function is very similar in form to the power law function in (21).

As an example, we illustrate the behavior of the wavelength dependent scattering observed on the Moon. *Hagfors and Evans* [1968] report angular scattering functions for observations of the moon at 3.6 cm, 23 cm, 68 cm, and 600 cm. We fit these functions using (20) and the Hagfors equation [*Hagfors and Evans*, 1968] to estimate quasi-specular slope values. In general, the Hagfors equation gave significantly better fits to these functions than (20). We plot the rms slopes inferred from the Hagfors fits (Hagfors $C^{-1/2}$) versus λ in Figure 9. To the extent that the Hagfors roughness represents the true surface topography, the best fit power law (21) implies a fractal dimension of ~2.2.

The apparent similarity between the wavelength dependent scattering behavior of the Moon and that derived for self-affine topography is highly suggestive, although by no means conclusive. There are complications that undoubtably arise due to diffuse (subwavelength scale) scattering and penetration into the regolith. If the lunar surface is self-affine and scatters purely through a quasi-specular mechanism, the Gaussian function (20) should have provided better fits to the angular scattering function than the Hagfors equation. Despite these difficulties, this is a promising area for future investigations.

4.3. Note on the Application of the Small Perturbation Model

The small perturbation model (SPM) is a group of radar scattering models which are commonly employed to study surfaces that deviate slightly from perfectly smooth [e.g., *Beckmann*, 1963; *van Zyl et al.*, 1991]. The model is considered limited to those surfaces with rms heights of

$$\sigma < \frac{\lambda}{20} \tag{22}$$

[*van Zyl et al.*, 1991]. In practice, little consideration is given to the length of the profile from which σ is measured. If, for example, the surface is oBn, rms heights measured along profiles 200 m long are ~3 times higher than those from 20-m profiles, which are, in turn ~3 times higher than 2-m profiles. If we assume that the length scale of the surface sampled by the radar is proportional in size to the wavelength, then rms heights measured along profiles should be scaled to this length. This has been instinctively known by many using the model; one practice is to use a high-pass filter on profiles, effectively limiting the profile length (B. Campbell personal communication, 1994). Many surfaces have probably been falsely ruled eligible or ineligible for the SPM based on (22) and rms heights from profiles of inappropriate length. Further work is needed to understand the relationship between wavelength and surface sampling size in this model. More generally, work is needed to determine the effects of non-stationary topography on these models.

5. Summary

The assumption of fractal topography explains several problems observed in the literature of surface roughness parameterization and planetary radar scattering. The adirectional slope distributions of surfaces measured by *McCollom and Jakosky* [1993] had nonzero means and modes, unlike the commonly assumed Gaussian or exponential distributions. Self-affine topography predicts this behavior in the form of a Rayleigh adirectional slope histogram. However, the adirectional slope density function utilized in quasi-specular models is a normalized (to solid-angle) histogram function. When suitably normalized, the Rayleigh histogram becomes a Gaussian adirectional slope density function with an rms slope equivalent to that found from a unidirectional profile.

The rms slope of the lunar surface inferred from multiwavelength radar measurements has been observed to decrease with increasing wavelength [*Muhleman*, 1964; *Hagfors and Evans*, 1968] and was found to have a power law dependence by *Simpson and Tyler* [1982]. We have shown that this behavior is consistent with fractal topography with fractal dimensions typical of many geologic surfaces measured on the Earth.

Finally, the small perturbation models applied to slightly rough surfaces usually place limits on the acceptable surface rms height, but no limits on the length over which this value is measured. If topography is self-affine over the scales assumed in this paper, then the rms height is a function of the profile length used to measure it. Therefore, we suggest that the length of the profile measured should be scaled to the radar wavelength; however, work is needed to determine this relationship and the more general effects of nonstationary topography on small perturbation models.

Acknowledgments. This work was supported by a Smithsonian Garber Fellowship to M.K.S. and NASA Planetary Geology and Geophysics Program grant NAGW-

1872 to Washington University. We are grateful to R. Simpson for thoroughly reviewing initial drafts of this paper, B. Campbell and H. Hastings for helpful discussions and comments, and L. Gaddis and an anonymous reviewer for constructive reviews.

References

Allan, D. W., Statistics of atomic frequency standards, *Proc. IEEE, 54*, 221-230, 1966.

Arvidson, R. E., M. A. Dale-Bannister, E. A. Guinness, S. H. Slavney, and T. C. Stein, Archive of geologic remote sensing field experiment data, Release 1.0, NASA Planet. Data Syst., Jet Propulsion Lab., Pasadena, Calif., 1991.

Austin, R. T., A. W. England, and G. H. Wakefield, Special problems in the estimation of power-law spectra as applied to topographical modeling, *IEEE Trans. Geosci. Remote Sens., GE-32*, 928-939, 1994.

Beckmann, P., Part 1-Theory, in *The Scattering of Electromagnetic Waves From Rough Surfaces*, edited by P. Beckmann and A. Spizzichino, MacMillan, New York, 1963.

Brown, S. R., and C. H. Scholz, Broad bandwidth study of the topography of natural rock surfaces, *J. Geophys. Res., 90*, 12,575-12,582, 1985.

Campbell, B. A, and J. B. Garvin, Lava flow topographic measurements for radar data interpretation, *Geophys. Res. Lett., 20*, 831-834, 1993.

Chase, C. G., Fluvial landsculping and the fractal dimension of topography, *Geomorphology, 5*, 39-57, 1992.

Efford, N. D., Characterization of the optical properties and surface roughnesses of atmosphereless planetary regoliths through photometric analysis, Ph.D. thesis, Lancaster University, Lancaster, England, 1990.

Falconer, K., *Fractal geometry: Mathematical Foundations and Applications*, John Wile, New York, 1990.

Farr, T., Microtopographic evolution of lava flows at Cima Volcanic Field, Mojave Desert,California, *J. Geophys. Res., 97*, 15,171-15,179, 1992.

Hagfors, T., and J. V. Evans, Radar studies of the Moon, in *Radar Astronomy*, edited by J. V. Evans and T. Hagfors, pp. 219-270, McGraw-Hill, New York, 1968.

Hastings, H. M., and G. Sugihara, *Fractals: A User's Guide for the Natural Sciences*, Oxford University Press, Oxford, 1993.

Huang, J., and D. L. Turcotte, Fractal mapping of digitized images: Application to the topography of Arizona and comparisons with synthetic images, *J. Geophys. Res., 94*, 7491-7495, 1989.

Huang, J., and D. L. Turcotte, Reply, *J. Geophys. Res., 95*, 5161, 1990.

Jupp, D. L. B., A. H. Strahler, and C. E. Woodcock, Autocorrelation and regularization in digital images, I, Basic theory,*IEEE Trans. Geosci. Remote Sens., GE-26(4)*, 463-473, 1988.

Mandelbrot, B. B., *The Fractal Geometry of Nature*, W. H. Freeman, New York, 1982.

Mark, D. M., and P. B. Aronson, Scale-dependent fractal dimensions of topographic surfaces: An empirical investigation, with applications in geomorphology and computer mapping, *Math. Geol., 16*, 671-683, 1984.

McCollom, T. M., and B. M. Jakosky, Interpretation of planetary radar observations: The relationship between actual and inferred slope distributions, *J. Geophys. Res., 98*, 1173-1184, 1993.

Muhleman, D. O., Radar scattering from Venus and the Moon, *Astron. J., 69*, 34-41, 1964.

Ogilvy, J. A., *Theory of wave scattering from random rough surfaces*, 277 pp., Institute of Physics Publishing, Bristol, England, 1991.

Power, W. L., and T. E. Tullis, Euclidean and fractal models for the description of rock surface roughness, *J. Geophys. Res.,96*, 415-424, 1991.

Sayles, R. S., and T. R. Thomas, Surface topography as a nonstationary random process, *Nature, 271*, 431-434, 1978.

Simpson, R. A., and G. L. Tyler, Radar scattering laws for the Lunar surface, *IEEE Trans. Antennas Propagat., AP-30*, 438-448, 1982.

Turcotte, D. L., *Fractals and Chaos in Geology and Geophysics*, Cambridge University Press, New York, 1992.

van Zyl, J. J., C. F. Burnette, and T. G. Farr, Inference of surface power spectra from inversion of multifrequency polarimetric radar data, *Geophys. Res. Lett., 18*, 1787-1790, 1991.

Voss, R. F., Fractals in nature: From characterization to simulation, in *The Science of Fractal Images* , edited by H. O. Peitgen and D. Saupe, pp. 21-69, Springer-Verlag, New York, 1988.

R. E. Arvidson and R. A. Brackett, Department of Earth and Planetary Sciences, Campus Box 1169, Washington University, One Brookings Drive, Saint Louis, MO 63130. (email arvidson@wunder.wustl.edu and brackett@wunder.wustl.edu)

M. K. Shepard, Department of Geography and Earth Science, Bloomsburg University, Bloomsburg, PA 17815. (email: shepard@planetx.bloomu.edu)

(Received November 30, 1994; revised January 23, 1995; accepted February 20, 1995.)